AD 740832

An Investigation of the Drag Forces on a Shaft Rotating Concentrically in a Porous Cylinder With Fluid Injection or Suction

BOBBY J. GAINES
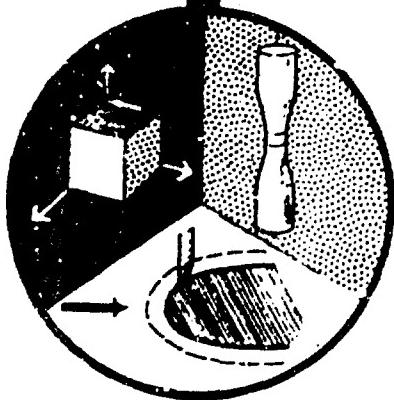
REPORT EM 72-2

DEPARTMENT OF ENGINEERING MECHANICS
THE UNIVERSITY OF TENNESSEE
KNOXVILLE, TENNESSEE 37916

MARCH 1972

D D C

MAY 1 1972

B

56

DOCUMENT CONTROL DATA - R & D

Security classification of title, body of abstract and indexing annotation must be entered when the overall report is classified)

1 ORIGINATING ACTIVITY (Corporate author)	2a. REPORT SECURITY CLASSIFICATION
The University of Tennessee Department of Engineering Mechanics Knoxville, Tennessee 37916	Unclassified
	2b. GROUP

3 REPORT TITLE

An Investigation of the Drag Forces on a Shaft Rotating Concentrically in a Porous Cylinder with Fluid Injection or Suction

4 DESCRIPTIVE NOTES (Type of report and inclusive dates)

Interim

5 AUTHOR(S) (First name, middle initial, last name)

Bobby J. Gaines

6 REPORT DATE	7a. TOTAL NO OF PAGES	7b. NO. OF REFS
March 1972	45	7

8a. CONTRACT OR GRANT NO	9a. ORIGINATOR'S REPORT NUMBER(S)
N00014-68-A-0144	EM 72-2
b. PROJECT NO	
c.	9b. OTHER REPORT NO(S) (Any other numbers that may be assigned this report)
d	

10 DISTRIBUTION STATEMENT

Distribution of this document is unlimited

11 SUPPLEMENTARY NOTES	12 SPONSORING MILITARY ACTIVITY

13 ABSTRACT

The equations of motion for steady incompressible flow in an annulus with fluid removal or injection at the porous walls have been reduced to a pair of ordinary differential equations by Terrill. Solutions for the case in which one wall rotates are not yet available; however, the solution of the related problem of a plane channel with a moving wall can be expressed in terms of the corresponding results for a stationary wall. That solutions is obtained in the present work. The solution is used to determine the drag on the moving wall. Preliminary experimental results with an apparatus consisting of a porous outer cylinder and a solid rotating shaft, sized such that the radius ratio is 0.926, indicate satisfactory agreement with the theoretical calculations for the case of fluid injection; however, there is poor agreement for the fluid removal case.

DD FORM 1473 (PAGE 1)

S/N 0101-807-6801

14. KEY WORDS	LINK A		LINK B		LINK C	
	ROLE	WT	ROLE	WT	ROLE	WT
Air bearings						
Channels - Flow						
Drag torque						
Dynamic seals						
Laminar Flow						
Porous walls						
Rotating boundaries						
Shaft seals						

The University of Tennessee

Department of Engineering Mechanics

Knoxville, Tennessee 37916

AN INVESTIGATION OF THE DRAG FORCES ON
A SHAFT ROTATING CONCENTRICALLY IN A POROUS
CYLINDER WITH FLUID INJECTION OR SUCTION

Bobby J. Gaines

FOREWORD

This document is submitted as an interim report covering work on transport mechanisms which is part of the Dynamic Sealing Research Program at the University of Tennessee, Knoxville. Support for this work was provided by Contract N00014-68-A-0144 with the Office of Naval Research.

This report was submitted to the University of Tennessee by Mr. B. J. Gaines in partial fulfillment of the requirements for the Master of Science Degree; it is presented here with minor changes in format.
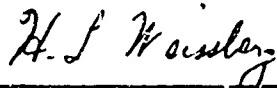
H L. Weissberg
Task Director
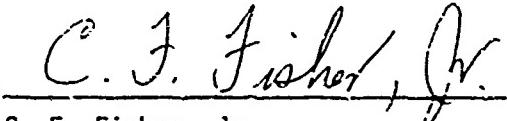
Approved: C. F. Fisher, Jr.
C. F. Fisher, Jr.
Program Manager

ACKNOWLEDGMENTS

ii

ABSTRACT

The equations of motion for steady incompressible flow in an annulus with fluid removal or injection at the porous walls have been reduced to a pair of ordinary differentia. equations by Terrill (3). Solutions for the case in which one wall rotates are not yet available; however, the solution of the related problem of a plane channel with a moving wall can be expressed in terms of the corresponding results (4, 5) for a stationary wall. That solution is obtained in the present work. The solution is used to determine the drag on the moving wall. Preliminary experimental results with an apparatus consisting of a porous outer cylinder and a solid rotating shaft sized such that the radius ratio is 0.926 indicate satisfactory agreement for the case of fluid injection; however, there is poor agreement for the fluid removal case.

TABLE OF CONTENTS

LIST OF FIGURES

LIST OF SYMBOLS

A	Average surface area of the porous cylinder
D	Viscous drag per unit area
$F(\lambda)$	Dimension function of the variable λ
$G(\lambda)$	Dimension function of the variable λ
J	Mass moment of inertia of shaft
K	Constant $= \mu W/h$
K_1	$2\pi r^3 \mu \ell / h$
L	Torque
R	The wall Reynolds numbers for the flow through the porous wall $\rho Vh/\mu$
T	Time interval between shaft rotational period measurements
T_a	Critical Taylor number
$\bar{\bar{U}}(0)$	Average value of the axial velocity at the fluid entrance
V	The radial velocity of the fluid at the porous cylinder surface
W	Tangential velocity at the shaft surface
h	Distance between the solid wall and the porous wall
ℓ	Shaft length
$\dot{m}$	Mass flow rate in 16 ib_m/sec
p	Fluid pressure
r	Shaft radius
t	Continuous time variable

vii

LIST OF SYMBOLS (Concluded)

u	Axial velocity component
v	Radial velocity component
w	Tangential velocity component
x	Axial coordinate
y	Radial coordinate
z	Tangential coordinate
α	Dummy variable
γ	Dummy variable
λ	y/h (dimensionless radial coordinate)
μ	Dynamic viscosity
ν	Kinematic viscosity
ρ	Fluid density
τ	Shaft rotational period — reciprocal shaft speed in sec/revolution
τ_0	Initial shaft rotational period
ω	Shaft angular velocity
ω_0	Initial shaft angular velocity

CHAPTER I

INTRODUCTION

This thesis covers an analytical study of the drag forces acting on a shaft rotating concentrically in a stationary porous cylinder, through which fluid is injected or withdrawn. The radius ratio of the annular section formed by the stationary porous cylinder and the rotating shaft is at least 0.9 in order that the annular section may be treated as a plane channel. Design of an experimental apparatus for testing the analytical study is also treated and preliminary experimental results are presented.

The study is restricted to the steady laminar, incompressible flow of a Newtonian fluid.

Previous work will be cited with numbers in parentheses which refer to the List of References.

A. Previous Work

A number of solutions for steady laminar flow in channels with porous walls have appeared in the literature over the past few years. A.S. Berman (1) presented the first solution to the Navier-Stokes equations for steady laminar flow in a uniformly porous channel. Berman (2) also gave a solution for the laminar steady-state flow of an incompressible fluid in an annulus formed by concentric uniformly porous cylinders for the special case where

the rate of fluid injection through one porous cylinder was equal to the rate of fluid withdrawal at the other porous wall. R. M. Terrill (3) reduced the problem of laminar flow through a porous annulus with constant suction velocity at the wall, and with swirl to the solution of four nonlinear differential equations. Terrill and Shrestha (4) investigated incompressible laminar flow in a channel with porous walls of different permeability and various combinations of flow rates through the walls. Most recently, M. S. Tsai (5) obtained solutions to the channel problem with one wall porous and to the annulus problem with one wall porous. Tsai used the perturbation method (1), method of averages (6), and numerical techniques to obtain solution for both the channel and annulus. He compared the results of the annulus and channel solutions and used the comparisons to determine the values of injection and suction rates and the annulus radius ratio for which the annulus may be treated as a flat channel.

Tsai's (5) results have been tested experimentally at the University of Tennessee by Dr. H. Weissberg and Mr. F. Curlee. The results indicate a good correlation between Tsai's study and the experimental data.

B. Present Work

The present work addresses the problem of extending Tsai's (5) investigation to the case of a rotating shaft, rather than a stationary one. Use is made of a plane channel approximation to get a novel solution of the Navier-Stokes equation for the tangential velocity distribution in an annulus with a

a porous outer wall. An apparatus design for testing the plane channel

approximation and preliminary experimental results are presented.

CHAPTER II

EQUATIONS OF MOTION

A. Assumptions and Equations

The following assumptions are made in treating the equations of motion for a shaft rotating within a porous cylinder:

1. The fluid flow is laminar, incompressible and fully developed.

2. The velocity of the fluid through the porous wall is independent of position.

3. The flow is axisymmetric; the shaft and porous cylinder are concentric.

Tsai's (5) results for a plane channel approximation to the annulus problem indicate that one may use the approximation, with less than 5-percent error in the calculated pressure drop, provided the radius ratio of the annulus section is greater than 0.9 and the wall Reynolds number for the plane channel is less than 2.0. The wall Reynolds number is defined as $R = \rho V h / \mu$; where V is the radial velocity of the fluid through the porous wall (positive for suction), h is the distance separating the plane solid wall from the plane porous wall, μ is the viscosity of fluid, and ρ is the mass density of the fluid.

4

Tsai's (5) plane channel approximation solution for the annular section was with a stationary solid wall. In the present work this approximation is generalized to treat the case of a concentrically rotating solid shaft. The rotating shaft, as shown in Figure 1, corresponds to a plane solid wall moving in a direction perpendicular to the average fluid motion.

A set of Cartesian coordinates is chosen for the plane channel approximation such that the x coordinate direction corresponds to the axial direction of the annulus section. The y direction corresponds to the radial direction of the annulus. The moving plane solid wall is physically located at y = 0 and corresponds to the surface of the shaft in the annular section. The z direction completes the right-handed orthogonal coordinate system indicated in Figure 1 and corresponds to the tangential velocity component of the shaft in the annular section.

The Navier-Stokes equations of motion for the steady, laminar, incompressible flow in the plane channel are

$$\rho \left(u \frac{\partial u}{\partial x} + v \frac{\partial u}{\partial y} + w \frac{\partial u}{\partial z} \right) = -\frac{\partial p}{\partial x} + \mu \left(\frac{\partial^2 u}{\partial x^2} + \frac{\partial^2 u}{\partial y^2} + \frac{\partial^2 u}{\partial z^2} \right) \tag{1}$$

$$\rho \left(u \frac{\partial v}{\partial x} + v \frac{\partial v}{\partial y} + w \frac{\partial v}{\partial z} \right) = -\frac{\partial p}{\partial y} + \mu \left(\frac{\partial^2 v}{\partial x^2} + \frac{\partial^2 v}{\partial y^2} + \frac{\partial^2 v}{\partial z^2} \right) \tag{2}$$

$$\rho \left(u \frac{\partial w}{\partial x} + v \frac{\partial w}{\partial y} + w \frac{\partial w}{\partial z} \right) = -\frac{\partial p}{\partial z} + \mu \left(\frac{\partial^2 w}{\partial x^2} + \frac{\partial^2 w}{\partial y^2} + \frac{\partial^2 w}{\partial z^2} \right). \tag{3}$$

6

COORDINATE	x	y	z
VELOCITY COMPONENT	u	v	w
AVERAGE AXIAL VELOCITY	$\bar{u}$		
SUCTION VELOCITY		V	
SOLID WALL VELOCITY			W

PLANE CHANNEL

FIXED UNIFORMLY POROUS WALL

MOVING SOLID WALL

ANNULUS

FIXED UNIFORMLY POROUS CYLINDER

SOLID ROTATING SHAFT
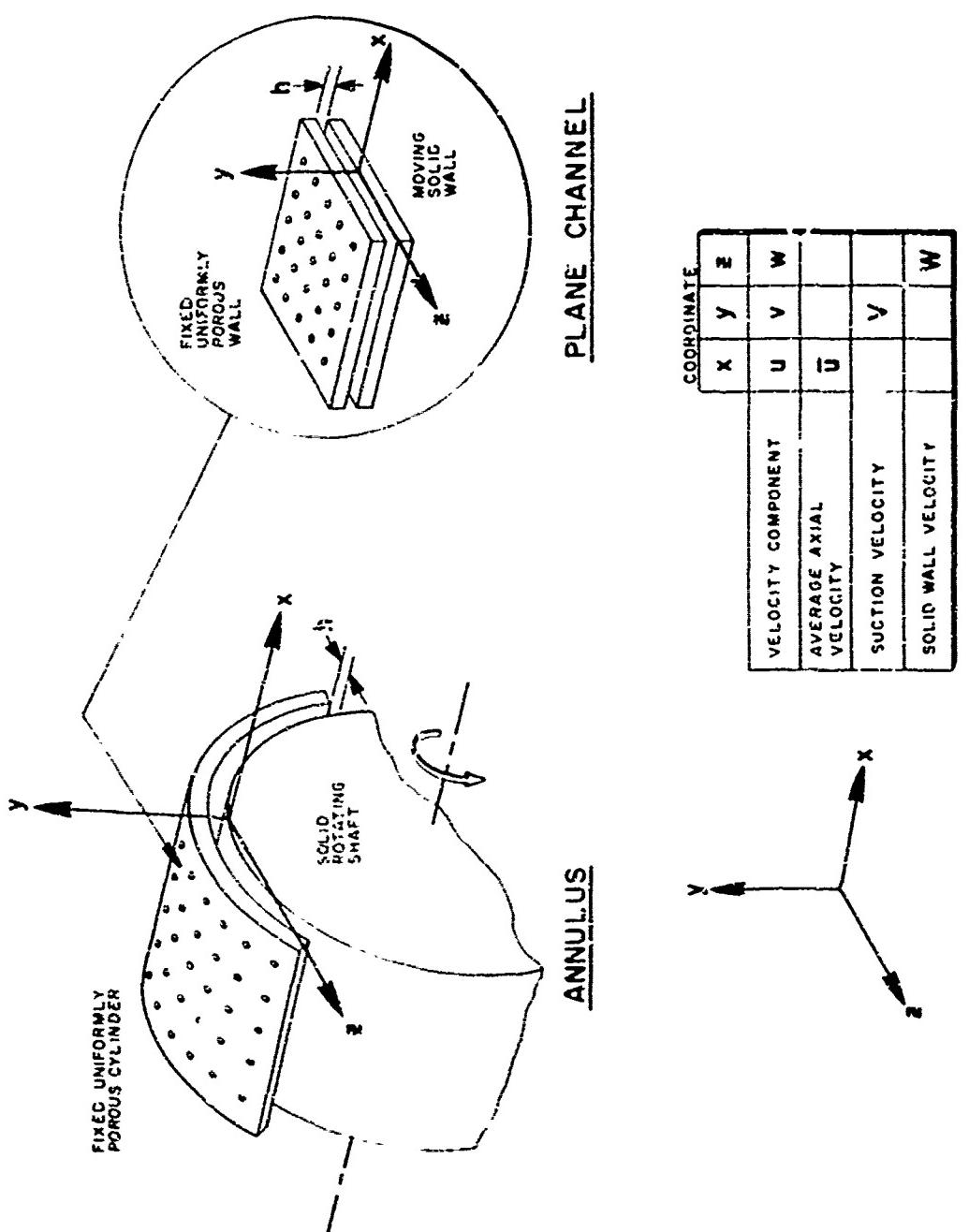
Figure 1. Plane channel approximation of annulus — coordinate system.

where u, v, and w are the fluid velocity components in the x, y, and z coordinate directions, respectively, and p is the fluid pressure.

The equation of continuity for an incompressible fluid is

$$\frac{\partial u}{\partial x} + \frac{\partial v}{\partial y} + \frac{\partial w}{\partial z} = 0 \ . \tag{4}$$

The axial velocity component u and the pressure p are assumed to be functions of the coordinates x and y only. This assumption is based on the shaft rotating concentrically in the porous cylinder; extending this to the plane channel approximation indicates that the distance h separating the stationary porous wall and the solid moving wall remains constant and independent of coordinate directions. The velocity at the stationary porous wall is assumed to be perpendicular to the wall with the constant[1] value V and the velocity component v is assumed to be a function of the y coordinate only.

The velocity component w in the z coordinate direction is also assumed to be a function of the coordinate y only. The assumptions are summarized as follows:

$$u = u \ (x, y).$$
$$p = p \ (x, y),$$
$$v = v \ (y),$$
$$w = w \ (y). \tag{5}$$

---

1. In practice the constant velocity through the wall was achieved by insuring that the pressure drop across the porous wall was much greater than the axial pressure drop in the annulus.

8

Substituting equation (5) into equations (1), (2), (3), and (4) leads, respectively, to

$$\rho \left(u \frac{\partial u}{\partial x} + v \frac{\partial u}{\partial y} \right) = -\frac{\partial p}{\partial x} + \mu \left(\frac{\partial^2 u}{\partial x^2} + \frac{\partial^2 u}{\partial y^2} \right) , \qquad (6)$$

$$\rho \left(v \frac{\partial v}{\partial y} \right) = -\frac{\partial p}{\partial y} + \mu \left(\frac{\partial^2 v}{\partial y^2} \right) , \qquad (7)$$

$$\rho \left(v \frac{\partial w}{\partial y} \right) = \mu \left(\frac{\partial^2 w}{\partial y^2} \right) , \qquad (8)$$

$$\frac{\partial u}{\partial x} + \frac{\partial v}{\partial y} = 0 \qquad . \qquad (9)$$

The boundary conditions are

$$u (x, 0) = 0, \quad v (0) = 0, \quad w (0) = W$$

$$u (x, h) = 0, \quad v (h) = V, \text{ and } w (h) = 0 \quad , \qquad (10)$$

where the velocity V is the injection or suction velocity at the porous boundary and W is the velocity of the moving wall.

Tsai (5) and Terrill (6) reduced equations (6) and (7) subject to equation (5) to the dimensionless ordinary differential equation

$$F'''' + R \left(F'F'' - FF''' \right) = 0 \quad , \qquad (11)$$

where F is a function of the dimensionless variable $\lambda = y/h$ and R is the wall

Reynolds number. The velocity components u and v are related to F and F' by

$$u(x, y) = \left(\overline{U}(0) - \frac{Vx}{h} \right) F'(\lambda)$$

and

$$v(y) = VF(\lambda) \quad , \quad (12)$$

where $\overline{U}(0)$ is the average velocity in the x direction at x = 0. The boundary

conditions on equation (11) are found by using equations (10) and (12).

$$F(0) = 0, \quad F(1) = 1$$

$$F'(0) = 0, \quad F'(1) = 0 \quad . \quad (13)$$

Now, in addition to solutions for 6 and 7, the solid moving wall

requires that a solution be found for equation (8). The velocity component in

the z coordinate direction is assumed to be of the form

$$w = WG(\lambda) \quad . \quad (14)$$

where W is the velocity of the solid wall and $G(\lambda)$ is a dimensionless function

of the variable λ. Substitution of equation (14) in (8) and use of (12) along

with the definition of wall Reynolds number $R = \frac{\rho h V}{\mu}$ yields

$$G''(\lambda) = R F(\lambda) G'(\lambda) \quad . \quad (15)$$

10

The boundary conditions on equation (15) are found from equation (14) and the no slip condition at the solid and porous walls:

$$G(0) = 1, \quad G(1) = 0. \tag{16}$$

The solution to equation (15) subject to the boundary conditions (16) is

$$G(\lambda) = 1 - \frac{\int_0^\lambda \exp\left(\int_0^\alpha RF'(\gamma)\,d\gamma\right)d\alpha}{\int_0^1 \exp\left(\int_0^\alpha RF(\gamma)\,d\gamma\right)d\alpha}. \tag{17}$$

It is interesting that the reduction of equations (6) and (7) to the dimensionless ordinary differential equation (11) is independent of the motion of the wall in the z coordinate direction; hence. the resulting velocity components in the x and y coordinate directions are valid. regardless of the motion of the wall in the z coordinate direction. However. equation (8) and its reduction to equation (15) are dependent on the solution to equation (11). It has thus been shown that the existing solutions of equation (11) can be incorporated into the new results, equation (17). to describe the case of shaft rotation and, indeed. this is the procedure that is used in the present work.

B. Equation for Viscous Drag

The shearing stress, i. e., drag force in the z direction per unit area of the moving wall, is

$$D = \mu\left(\frac{\partial w}{\partial y} + \frac{\partial v}{\partial z}\right)_{y=0} \tag{18}$$

Equations (5) and (14) are substituted into equation (18) to yield

$$D = \mu \frac{WG'(0)}{h} = KG'(0),\qquad (19)$$

where the constant K is defined as

$$K = \mu \frac{W}{h}.\qquad (20)$$

The expression for $G'(0)$ is found from equation (17) so that equation (19) may be written as

$$D = \frac{K}{\displaystyle\int_0^1 \exp\left(\int_0^\alpha RF(\gamma)\,d\gamma\right)d\alpha}\qquad (21)$$

It is interesting to take a closer look at equation (21). The case of no flow through the porous wall, $R = 0$, corresponds to the value unity for the denominator; hence, the ratio of the drag forces without flow to the drag forces with flow through the wall is just the value of the denominator of equation (21), that is $1/G'(0)$.

The viscous drag forces acting on a rotating shaft may be determined experimentally by measuring the time rate of change of angular velocity provided that all external forces are limited to those associated with viscous drag. An expression for angular momentum decay is

$$L = -J\frac{d\omega}{dt},\qquad (22)$$

where L is the applied torque or, in this case, the product of the viscous force and the moment arm, J, is the mass moment of inertia and ω is the

12

angular velocity. Equation (19) is the expression for the viscous drag force per unit area and may be converted to an expression for the drag torque by the appropriate introduction of shaft area exposed to the viscous drag and the moment arm; hence,

$$L = DAr , \qquad (23)$$

where A is the shaft surface area and r is the shaft radius. Equation (23) may be expanded to

$$L = \left(\frac{\mu W}{h}\right)\left(2\pi r\ell\right)\left(r\, G'(0)\right) . \qquad (24)$$

However, W is the velocity of a point on the shaft and is

$$W = r\omega , \qquad (25)$$

where ω is the angular rate of the shaft. Equations (25) and (24) combined become

$$L = K_1\, G'(0)\,\omega . \qquad (26)$$

where

$$K_1 = \frac{2\pi\, r^3 \ell \mu}{h} .$$

Since equations (22) and (26) are both expressions for the shaft torque due to viscous forces, they may be combined to yield

$$K_1 G'(0)\,\omega = -J\frac{d\omega}{dt} . \qquad (27)$$

Equation (27) is subject to

$$\omega = \omega_0 \text{ at } t = 0 \quad , \tag{28}$$

where ω_0 is the angular rate at the start of any rundown.

A solution to equation (27) subject to the boundary condition (28) is

$$\ell n \, \frac{\omega}{\omega_0} = -\frac{K_1 \, G'(0)}{J} \, t \quad . \tag{29}$$

In terms of the time period per revolution, $\tau = 2\pi/\omega$, equation (29) may be written as

$$\ell n \, \frac{\tau_0}{\tau} = -\frac{K_1 \, G'(0)}{J} \, t \quad , \tag{30}$$

where τ_0 is the initial time period for one revolution of the shaft and τ is a continuous variable which expresses the period at any subsequent time. Equation (30) provides the basis for the experimental work to be discussed in the next chapter.

CHAPTER III

EXPERIMENTAL WORK

The objective of the experimental part of the work is to make a preliminary investigation into the validity of using the previously discussed plane channel approximation in solving the Navier-Stokes equations for a solid shaft rotating in a porous sleeve. The equipment described in Tsai's (5) investigation was available for this work; however, modifications were necessary to provide for rotation of the shaft. The experimental apparatus was modified accordingly and is described below.

Our experimental test of the present theoretical work consisted of using the rundown history of a rotating shaft to obtain experimental values of $G'(0)$ from equation (30). That work is also described in this chapter.

A. Apparatus

In the following description of the test equipment, reference is made to the diagram of the apparatus (Figure 2) and the lettered parts designated on the diagram.

The ends of the porous sintered titanium cylinder (E) are attached to the flanges (F) and (G) at the epoxy joints (J). These flanges are attached to flanges (R) and (L), thus mounting the porous cylinder inside the jacket [H].

15
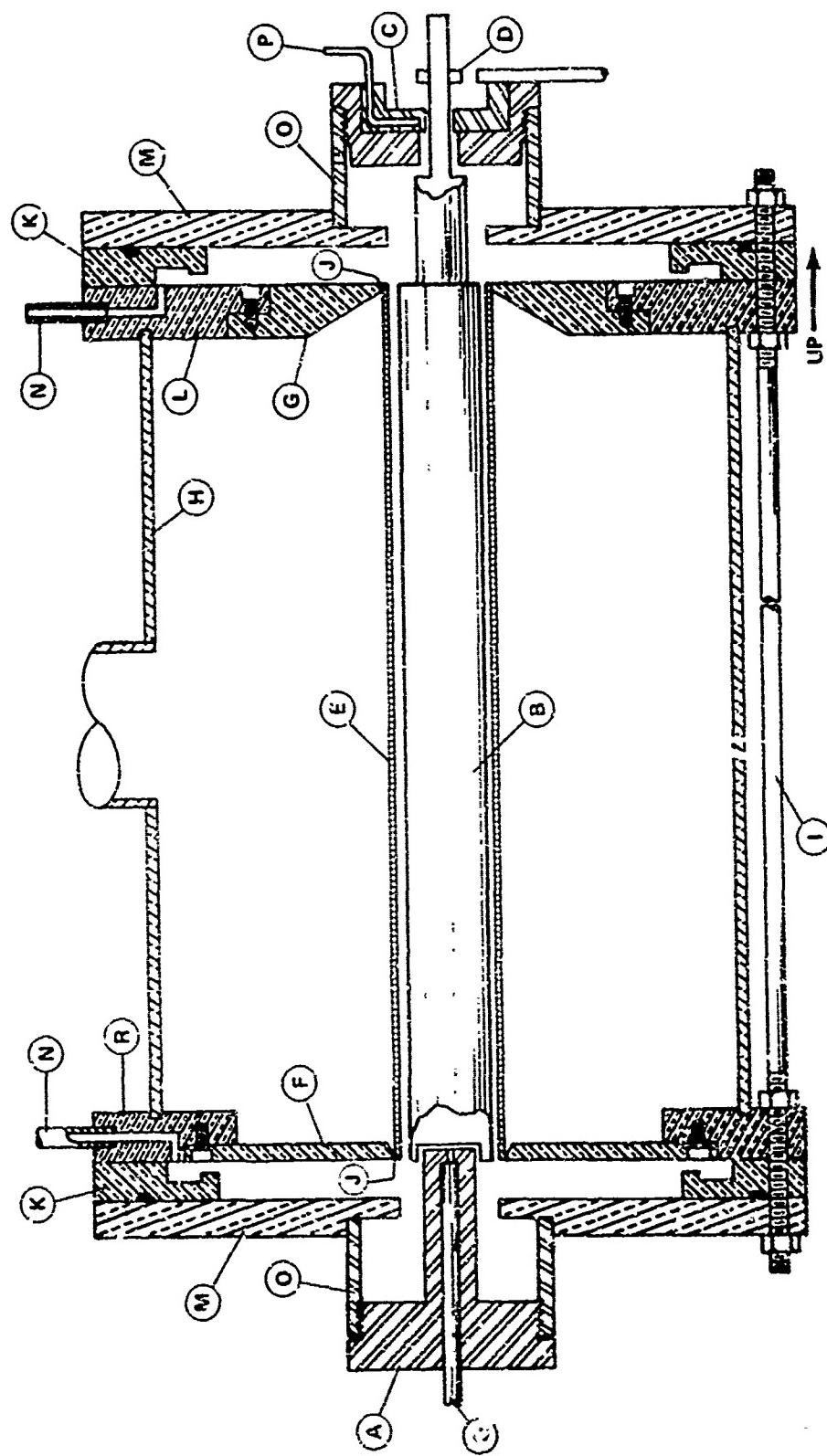
Figure 2. Diagram of apparatus.

which is used to supply air or to remove it from the outside of the porous

cylinder. Three rods (i), equally spaced around the flanges are used to pro-

tect the thin joints (J) from rupture in case of exposure to excessive air pres-

sure in the jacket.

The rotating shaft (B) is supported in the vertical direction by the gas

thrust bearing (A). Thrust bearing (A) also offers some lateral support.

The uppermost part of the rotating shaft is supported radially by gas bearing

(C). Both gas bearings (A) and (C) help maintain a concentric condition of

the rotating shaft (B) and the stationary porous cylinder (E).

The annular channel consists of the space between the rotating shaft

(B) and the porous cylinder (E). Calming chambers are provided by the

spacers (K) between the flanges (M) and (R) and (M) and (L). The cham-

bers are used for calming the air entering or being discharged. There are

thus five flow paths through which the airstream can enter or leave the annular

channel: the port located in the center of jacket (H), the two ports (not

shown) passing through the spacer rings (K) into the calming chambers at

each end, and the gas bearings (A) and (C). The two ports labeled (N) are

used for monitoring the pressure in the calming chambers.

Rotating shaft (B) is actuated by turbine (D) and two jets not shown.

The shaft is constructed of aluminum and is machined both outside diameter

and inside diameter. The shaft provides a radial gap of 0.0528 in. The

radius ratio for this shaft and the porous cylinder (E) is 0.9263. The shaft

(B) wall thickness is small in order to keep the inertia to a small value and, hence, makes the effects of the viscous drag more pronounced.

The bottom gas bearing fed by (Q) and the top gas bearing fed by (P) were designed to give minimum drag. The gas bearing drag and end effects were calculated to be less than three percent of the maximum drag anticipated.

Shaft speed is determined by utilizing a dark spot on the shaft, a Mechanical Technology, Inc., Fotonic sensor and two Hewlett-Packard time interval counters. The Fotonic sensor generates one pulse per revolution of the shaft. The two Hewlett-Packard counters are used to measure the time for one complete revolution of the shaft and the time between shaft period measurements. The shaft rundown history is obtained by recording the counter readings.

B. Description of Experiments

Tests were run with filtered dry air as the test fluid for wall Reynolds numbers ranging from +3.359 to -5.241. Mass flow rates through the porous wall were adjusted and the wall Reynolds numbers were calculated from these rates and the laboratory conditions. An example of these calculations is shown in the Appendix. The calculated wall Reynolds numbers were used with Tsai's (5) perturbation method to provide values of F in equations (17). The results were used to determine the theoretical value of the denominator of equation (21) and, hence, $G'(0)$ for the flow conditions imposed during the experiments.

18

The experiments and data acquisition were designed to obtain an accurate graph of equation (30) $\ln \frac{T_0}{T}$ versus time for wall Reynolds numbers corresponding to those used in the analytical determination of $G'(0)$.[2] Accurate measurements of shaft rotational period and elapsed time were accomplished with precise electronic counters and a shaft rotation sensing device, as described previously. The mass flow rates into the test apparatus were accounted for with calibrated critical orifices and electronic mass flow meters. Fluid temperature, room temperature and atmospheric pressure were monitored during the testing and were used in the calculations for mass flow rates, fluid viscosity and wall Reynolds numbers. Tests were run with no mass flow through the porous wall, mass flow outward and mass flow inward. These conditions are described on the following pages.

Positive Reynolds Numbers

Positive wall Reynolds numbers correspond to the case when fluid is allowed to flow radially outward through the porous cylinder (E) in Figure 2 (p. 15). The fluid entered the system through bottom bearing and was monitored with a mass flow meter. The various wall Reynolds numbers were obtained with a calibrated critical orifice to control the flow into the bottom port (N). The fluid entered the annular section at the bottom and flowed

---

2. The equation predicts that such a graph should be linear with its slope equal to $-K_1 G'(0)/T$.

axially and radially outward into the jacket (H), which was maintained at atmospheric pressure. The fluid flowing out of the jacket (H) was monitored with a mass flow meter to insure that only the fluid flowing into the annulus section at the bottom flowed axially and radially through the porous cylinder (E). Fluid flow to the top bearing was discharged through a resistance at port (N) and was adjusted to insure that no fluid from the top bearing entered the annular section at the top.

Negative Reynolds Numbers

Negative wall Reynolds numbers correspond to fluid flow into the jacket (H, (Figure 2, p. 15) and through the porous cylinder (E) into the annulus formed by porous cylinder (E) and shaft (B). The fluid was discharged through top port (N) and ports in the top bearings support. Fluid for the bottom bearing was withdrawn from the bottom calming chamber at bottom port (N) and was monitored with a mass flow meter to insure that only fluid for the bottom bearing was discharged at bottom port (N). A calibrated critical orifice controlled the flow entering the jacket (II).

Zero Reynolds Number

The zero wall Reynolds number corresponds to zero induced fluid flow in the annular section formed by shaft (B) and porous cylinder (E) in Figure 2. Fluid from the bottom thrust bearing was discharged at bottom port (N). Fluid for the top bearing was vented through ports in the bearing support

plate and also through top part (N). The jacket (H) was closed to insure that no fluid flowed through the porous cylinder (E). With this arrangement there is also no axial flow. The pressure inside the jacke' (H) and calming chambers at each end of the apparatus was monitored to insure that it was atmospheric.

The test procedure for all three flow conditions was as follows:

1. The flow conditions were adjusted to obtain a desired wall Raynolds number. Calibrated critical orifices and electronic mass flow meters along with flow restrictors were utilized to accomplish the desired flow condition for each experimental run. The shaft was rotated slowly during the flow adjustments to insure a concentric relationship between the shaft (B) and porous cylinder (E) of Figure 2 (p. 15). The fluid temperature, room temperature. and barometric pressure were observed and recorded for each experimental run.

2. The shaft was rotated and allowed to stabilize. All controllable external torques were removed so that only the viscous drag imposed by the flow conditions remained. The shaft speed decay measurements were initiated using one Hewlett-Packard counter to measure the time period of one complete revolution of the shaft and another to measure elapsed time. The successive period measurements and elapsed time were made using the gate closing pulse of the time period counter to actuate the second counter in a time interval mode. The manually opened gate of the time period counter

stopped the time interval counter and closing of the gate after one complete revolution of the shaft started the time interval counter for another elapse time measurement. The operation of the counters in this manner allowed the time period per revolution and elapsed time between period measurements to be determined with an accuracy of $100\,\mu\text{sec}$. The manual selection of the automatic timing sequence allowed the operator ample time to record the shaft period and elapsed time before starting the next sequence. This procedure resulted in 10 to 20 sec between shaft period measurements. The total time elapsed for any experimental run was from 200 to 300 sec. The shaft speed at the beginning of the test runs ranged from about 200 to 300 rpm.

3. Each flow condition was tested with the shaft rotating first in the clockwise direction and then in the counterclockwise direction. This insured that any asymmetry associated with rotational direction would be duly noted.

C. Experimental Data Treatment

The objective in the treatment of the raw data is to generate an accurate shaft speed variation with time such that an experimental graph of equation (30) can be obtained for each flow condition.

The output of the shaft rotation sensing device is typically a square wave electrical signal as indicated in Figure 3. The raw data from the experimental runs are the τ's and T''s indicated in the figure. The determination of the c's also indicated in the figure, is necessary in order to get an
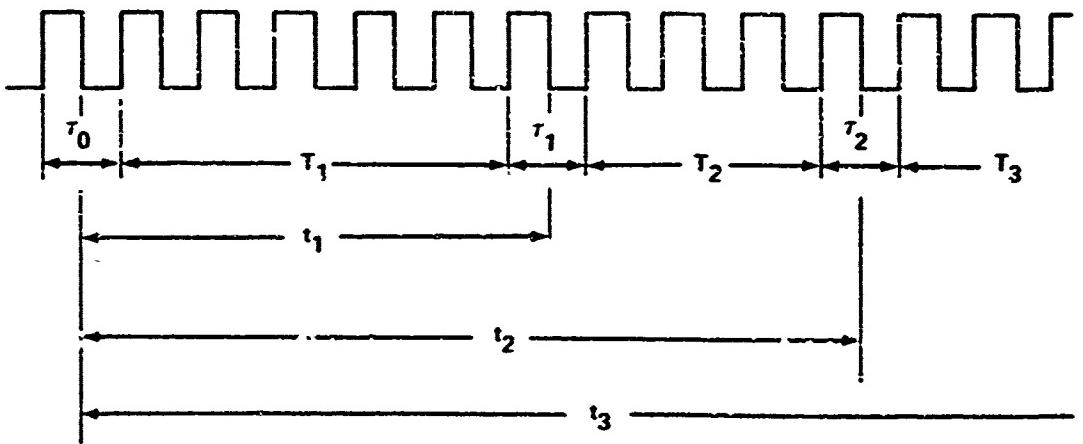
Figure 3. Fotonic sensor waveform and timing scheme.

accurate graph of the shaft speed variation with time. Figure 3 shows that

$$t_n = \sum_{i=1}^{n} \left[1/2 \left(\tau_{i-1} + \tau_i \right) + T_i \right] \ . \tag{31}$$

A small computer was used to obtain values of t_n from equation (31) and to compute the corresponding left side of equation (30). The determination of the mass moment of inertia J, which appears in equation (30), is discussed in the Appendix.

A regression analysis was used to fit a straight line to the data $\ln \tau_0/\tau$ versus time for each experimental run. This procedure gives the slope and intercept of the fitted line and also the coefficient of a 95-percent confidence interval for these two statistical parameters.

The t-distribution was used for the 95-percent confidence interval determination. This was based on the generally accepted value of 30 data points above which the normal distribution is used and below which the t-distribution is used. Most of the experimental runs in the present work contained less than 30 data points.

D. Results

The experimental values for $G'(0)$ were obtained from equation (30) using the experimental slopes to obtain values of $-K_1 G'(0)/J$. The slopes were deter .ined from a least squares straight line fit of the experimental data as previously explained. The right side .f equation (30) represents the slope and the time variable t; hence, the coefficient of t was set equal to the slope and the drag ratio. $G'(0)$, was calculated for each experimental run. A typical example of this calculation is shown in the Appendix.

A total of 36 experimental runs were made at nine different wall Reynolds numbers. Table I is a comparison of the theoretical and experimental results for the 36 runs. Repeatability of the data was good within 5 percent for more than one run at the same wall Reynolds number. Several different runs were made on different days at wall Reynolds numbers equal to zero and Table I indicates that the repeatibility is excellent.

Figures 4 through 12 illustrate typical runs for various Reynolds numbers. Each figure shows the theoretical line calculated from equation

TABLE I

TABULATION OF THEORETICAL AND EXPERIMENTAL RESULTS

| Run No.	Wall Reynolds No.	Theoretical Slope	Experimental Slope and 95% Confidence Limits		Theoretical $G'(\omega)$	Experimental $G'(\omega)$	
			Clockwise	Counterclockwise		Clockwise Rotation	Counterclockwise Rotation
47-1 -2	0.0000	-0.0025	-0.0031 ± 0.000019	-0.0031 ± 0.000032	1.0000	1.3435	1.3639
44-3	0.0000		-0.0031 ± 0.000019	-0.0034 ± 0.000050			
55-1 -2	0.0000		-0.0031 ± 0.000023	-0.0034 ± 0.000017			
56-1 -2	0.0000		-0.0031 ± 0.000031				
49-1/-2	-0.9244	-0.0032	-0.0035 ± 0.000004	-0.0035 ± 0.000018	1.3013	1.3039	1.4039
49-3	-0.9238	-0.0032		-0.0035 ± 0.000046	1.3013		1.4039
50-1/-2	-1.8496	-0.0039	-0.0039 ± 0.000034	-0.0039 ± 0.000034	1.5533	1.5643	1.5846
51-1/-2	-3.0127	-0.0046	-0.0045 ± 0.000023	-0.0042 ± 0.000015	1.8275	1.8050	1.7248
51-3			-0.0045 ± 0.000012			1.6050	
54-1/-2			-0.0047 ± 0.000008	-0.0043 ± 0.000006		1.8852	1.7658
54-3			-0.0046 ± 0.000120			1.8451	
52-1/-3	-4.1617	-0.0051	-0.0051 ± 0.000022	-0.0046 ± ---------	2.0295	2.0296	1.8452
52-2	-4.1617	-0.0051	-0.0051 ± 0.000032		2.0295	2.0296	
53-1/-2	-5.2407	-0.0055	-0.0059 ± 0.000055	-0.0048 ± 0.000170	2.2095	2.3289	1.9253
53-3			-0.0058 ± 0.000036			2.3289	
53-4			-0.0060 ± 0.000210			2.4092	
58-2/-2	+1.0466	-0.0014	-0.0030 ± 0.000102	-0.0039 ± 0.000148	0.6236	1.4452	1.5656
58-3	+1.0466	-0.0016	-0.0036 ± 0.000068		0.6226	1.4452	
59-1/-2	+2.1255	-0.0007	-0.0039 ± 0.000159	-0.0047 ± 0.000060	0.2909	1.5656	1.8868
59-3	+2.1255	-0.0007	-0.0039 ± 0.000143		0.2909	1.5656	
60-1/-2	+3.3587	-0.0002	-0.0039 ± 0.000084	-0.0051 ± 0.000026	0.0840	1.5656	2.0273
60-3	+3.3587	-0.0002		-0.0050 ± 0.000051	0.0840		2.0273
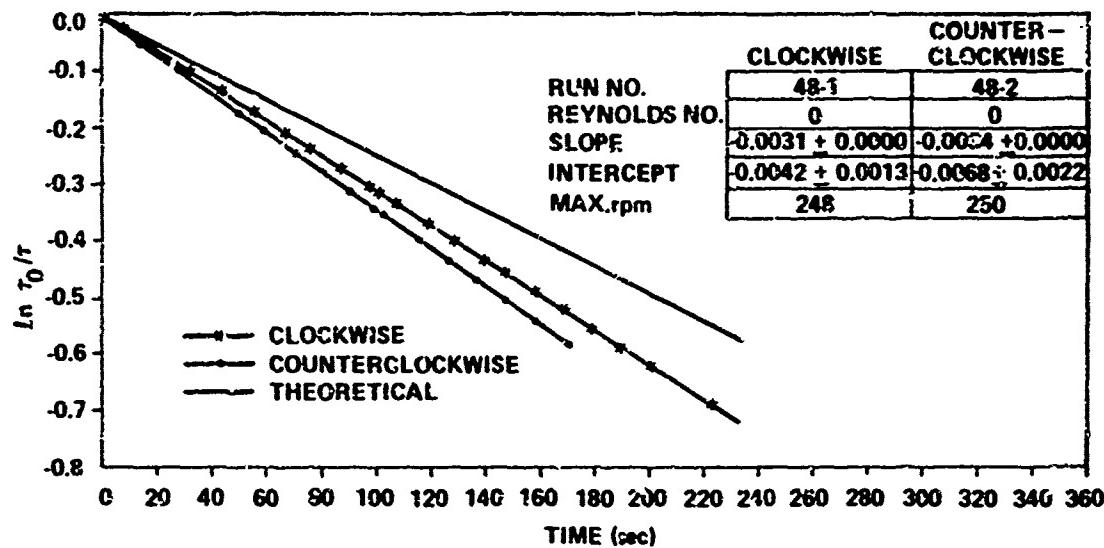
Figure 4. Shaft speed decay, R = 0.

	CLOCKWISE	COUNTER- CLOCKWISE
RUN NO.	48-1	48-2
REYNOLDS NO.	0	0
SLOPE	-0.0031 ± 0.0000	-0.0034 ± 0.0000
INTERCEPT	-0.0042 ± 0.0013	-0.0068 ± 0.0022
MAX.rpm	248	250
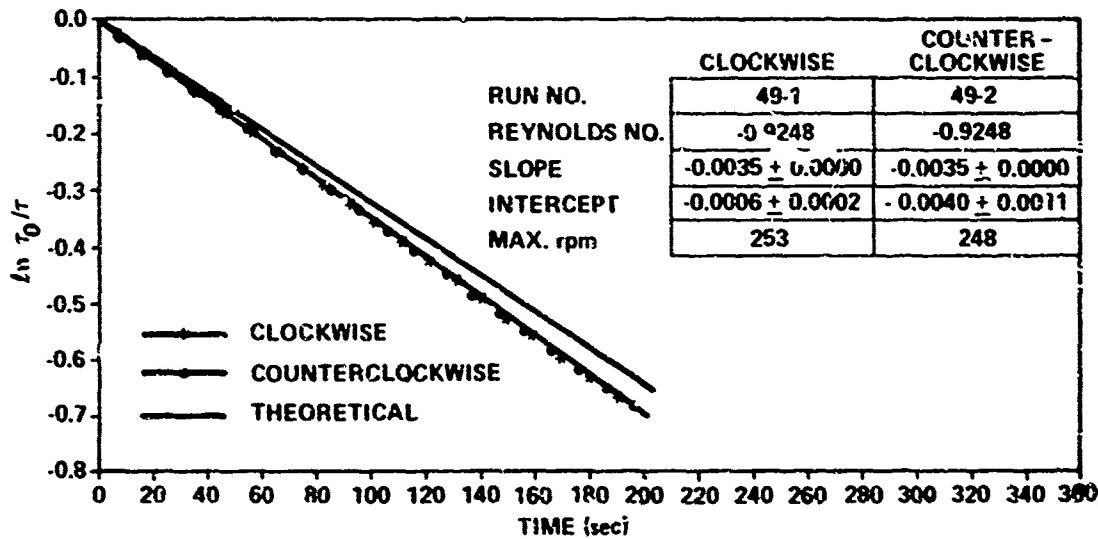
Figure 5. Shaft speed decay. R = -0.9248.

	CLOCKWISE	COUNTER- CLOCKWISE
RUN NO.	49-1	49-2
REYNOLDS NO.	-0.9248	-0.9248
SLOPE	-0.0035 ± 0.0000	-0.0035 ± 0.0000
INTERCEPT	-0.0006 ± 0.0002	-0.0040 ± 0.0011
MAX. rpm	253	248

	CLOCKWISE	COUNTER-CLOCKWISE
RUN NO.	50-1	50-2
REYNOLDS NO.	-1.8496	-1.8496
SLOPE	-0.0039 ± 0.0000	-0.0039 ± 0.0000
INTERCEPT	-0.0030 ± 0.0019	+0.0020 ± 0.0018
MAX. rpm	250	244
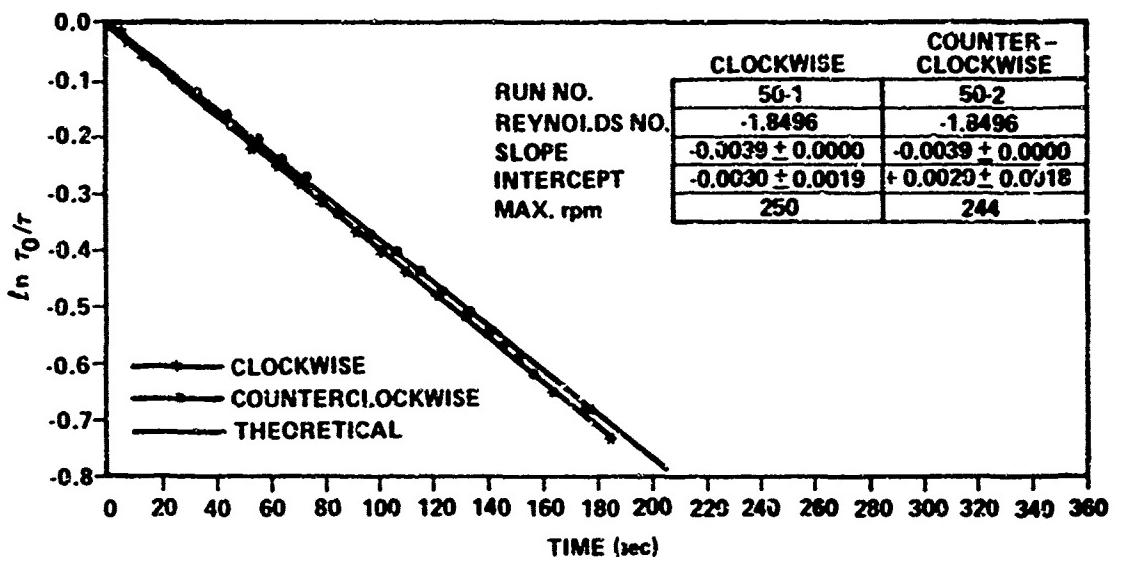
Figure 6. Shaft speed decay, R = -1.8496.

	CLOCKWISE	COUNTER-CLOCKWISE
RUN NO.	51-1	51-2
REYNOLDS NO.	-3.0827	-3.0827
SLOPE	-0.0045 ± 0.0000	-0.0042 ± 0.0000
INTERCEPT	-0.0029 ± 0.0011	-0.00⁻0 ± 0.0008
MAX. rpm	252	251
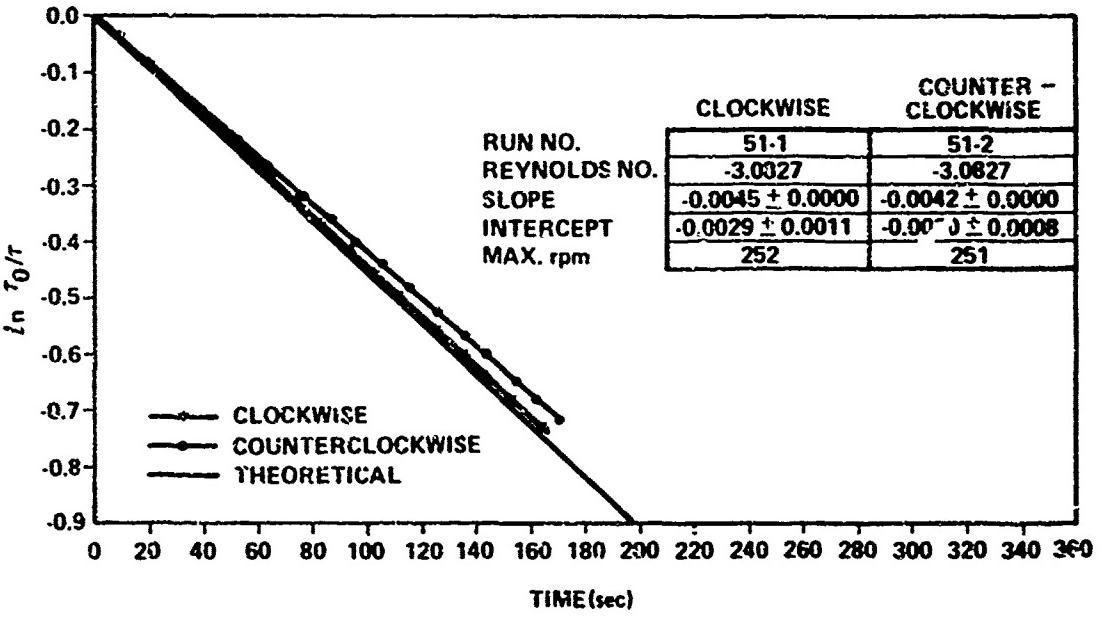
Figure 7. Shaft speed decay. R = -3.0827.

	CLOCKWISE	COUNTER–CLOCKWISE
RUN NO.	52-1	52-3
REYNOLDS NO.	-4.1617	-4.1617
SLOPE	-0.0051 ± 0.0000	-0.0046 ± 0.0000
INTERCEPT	-0.0001 ± 0.0005	-0.0027 ± 0.0014
MAX. rpm	241	243

— CLOCKWISE
— COUNTERCLOCKWISE
— THEORETICAL
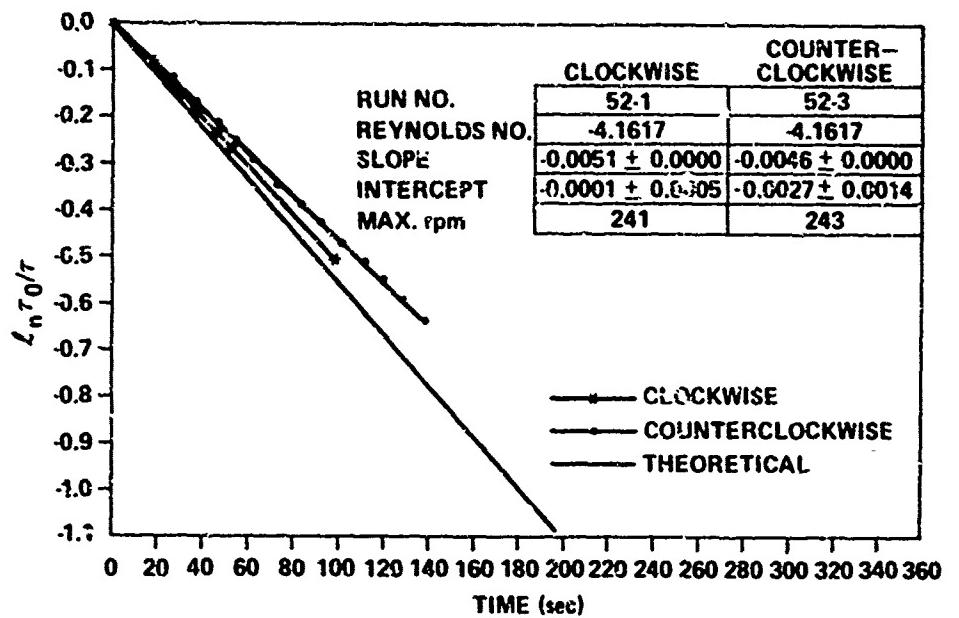
Figure 8. Shaft speed decay, $R = -4.1617$.

	CLOCKWISE	COUNTER–CLOCKWISE
RUN NO.	53-1	53-3
REYNOLDS NO.	-5.2407	-5.2407
SLOPE	-0.0058 ± 0.0001	-0.0048 ± 0.0002
INTERCEPT	-0.0025 ± 0.0011	-0.0220 ± 0.0059
MAX. rpm	223	222

— CLOCKWISE
— COUNTERCLOCKWISE
— THEORETICAL
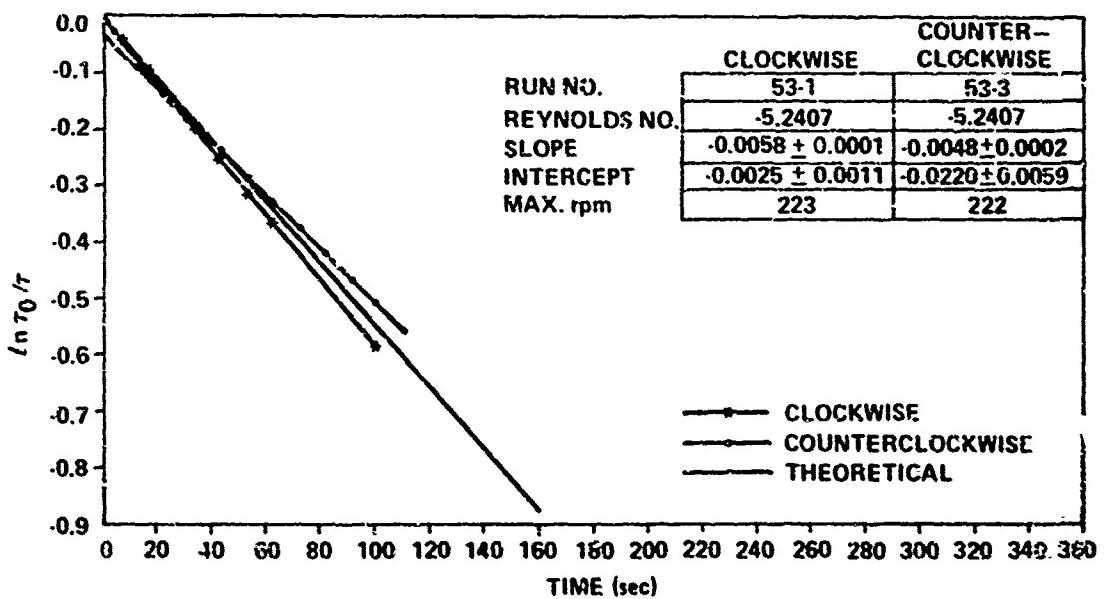
Figure 9. Shaft speed decay, $R = -5.2407$.

	CLOCKWISE	COUNTER–CLOCKWISE
RUN NO.	58-3	58.2
REYNOLDS NO.	+1.0466	+1.0466
SLOPE	-0.0036 + 0.0001	-0.0040 ± 0.0001
INTERCEPT	-0.0041 ± 0.00?8	-0.0241± 0.0087
MAX. rpm	270	248
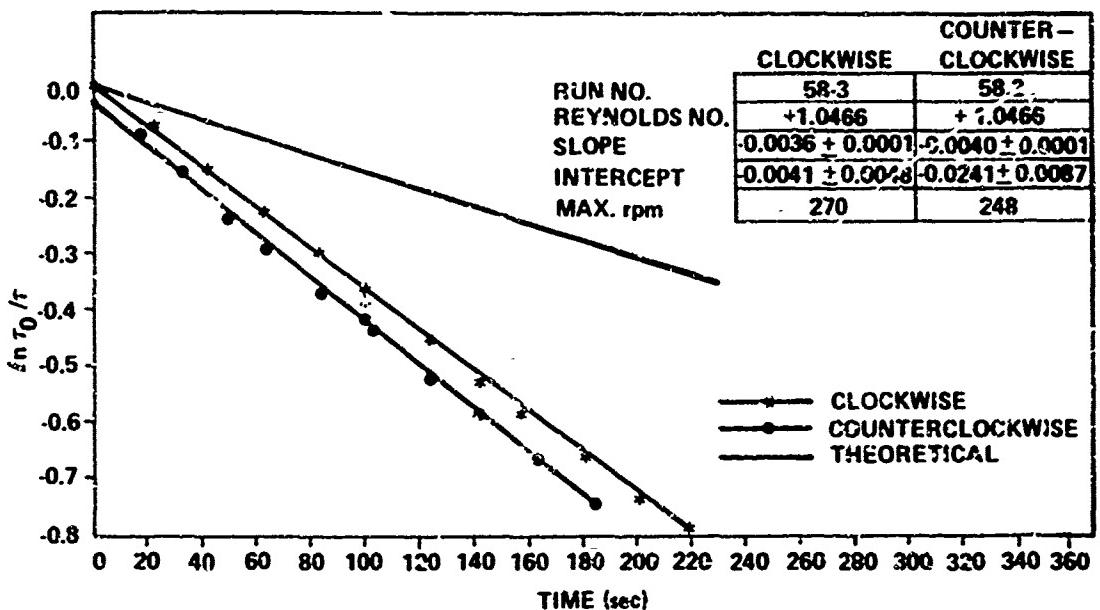
Figure 10. Shaft speed decay, $R = +1.0466$.

	CLOCKWISE	COUNTER–CLOCKWISE
RUN NO.	59-1	59-2
REYNOLDS NO.	+2.1255	+2.1255
SLOPE	-0.0039 + 0.0002	-0.0046 + 0.0001
INTERCEPT	-0.0063 + 0.0102	+ 0.X060 + 0.0038
MAX. rpm	266	264
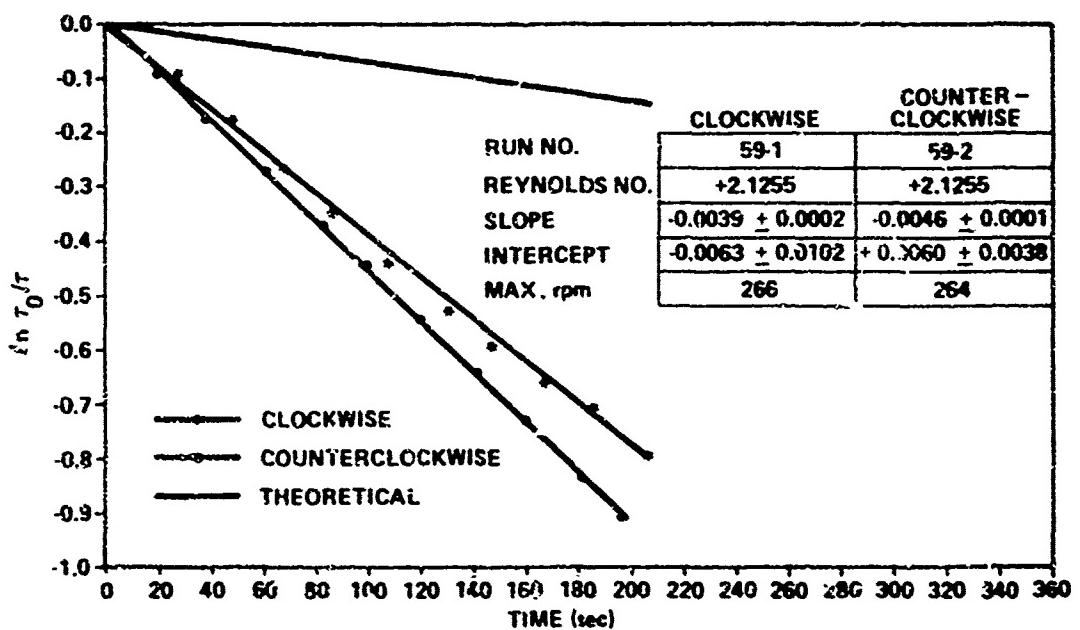
Figure 11. Shaft speed decay, $R = +2.1255$.
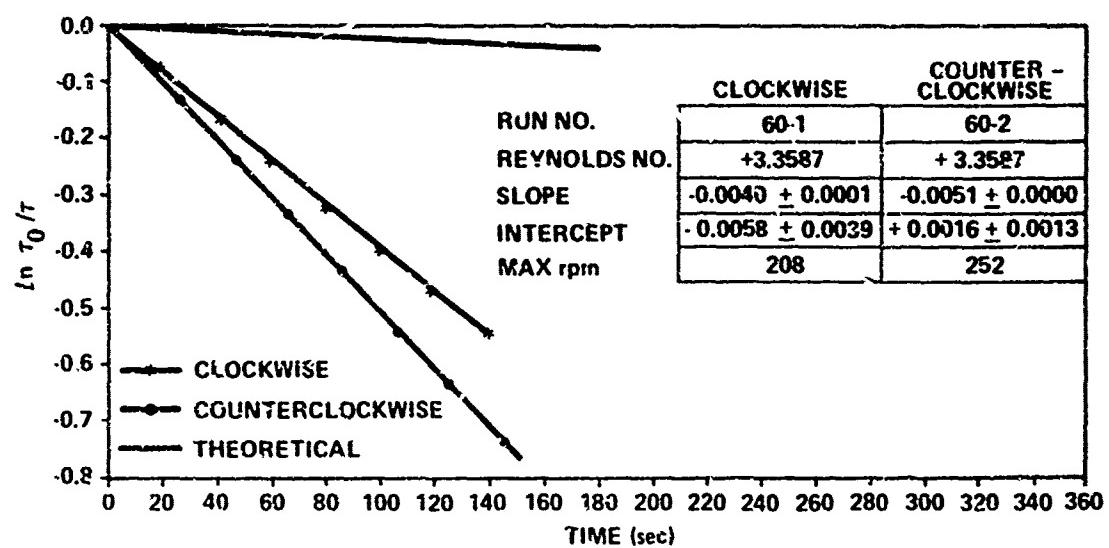
Figure 12. Shaft speed decay, R = +3.3587.

(30) and the least squares line as fitted through the plotted experimental

points. There are two such experimental lines because data were taken for

two directions of rotation as explained in a previous section. Description of

Experiments. A table inserted in each figure also provides the following in-

formation:

1. The wall Reynolds number for the run.

2. The least squares intercept and its deviation (95-percent confi-

dence interval) for each direction of shaft rotation.

3. The least squares slope and its deviation (95-percent confidence

interval) for each direction of shaft rotation.

4. The shaft speed at the beginning of data acquisition.

The results of the experimental runs are conveniently summarized by

plotting the theoretical (see section on Viscous Drag) and experimental values

(Table I, p. 24) of the drag ratio G' (0), versus wall Reynolds numbers; such

a plot is shown in Figure 13. The computed values of G' (0) are given for

both clockwise and counterclockwise shaft rotation directions. Reasonably

good agreement[3] between the theoretical and experimental values of G' (0) is

indicated for clockwise shaft rotation with wall Reynolds numbers from -1 to

-5; the range of reasonable agreement for counterclockwise shaft rotation

extends from -1 to -3. Examination of Figures 5, 6, and 7 (pp. 25-26) indi-

cates that the slope for both rotating directions in the wall Reynolds number

---

3. A statistical test of the experimental data is discussed in the appendix.
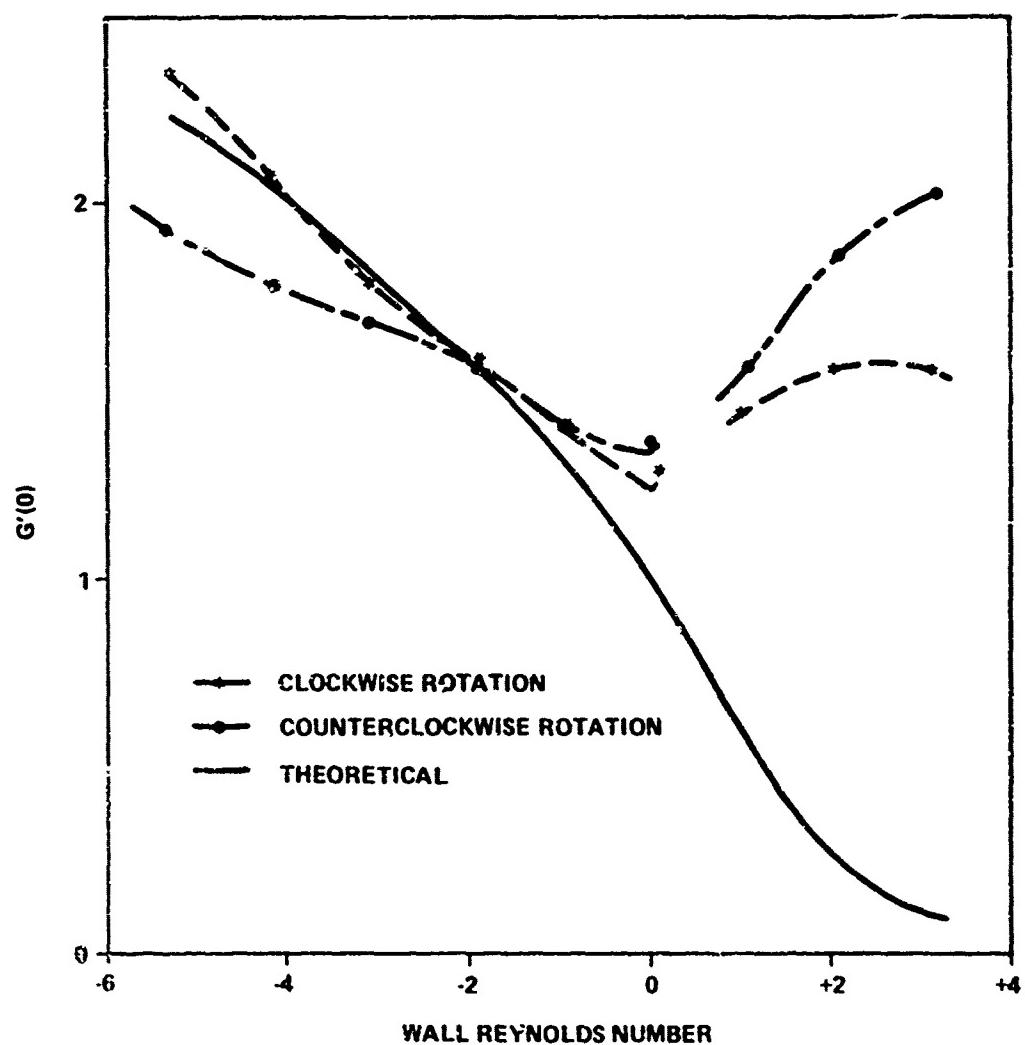
Figure 13. Theoretical and experimental drag ratios.

range -1 to -3 are within 10 percent of each other. Positive wall Reynolds numbers resulted in no apparent agreement between the theoretical and experimental results. This lack of agreement is quite evident in Figure 13. A discussion of this is given below.

E. Discussion

The lack of agreement between the theoretical predictions and the experimental results noted above suggest that an instability may exist for positive wall Reynolds numbers. During the experimental runs with positive wall Reynolds numbers, it was observed that a slight induced vibration of the apparatus would cause the shaft to become unstable[4] and to stop (because of contact between the shaft and either of the bearing stops) in a few revolutions. This is thought to be associated with the stiffness of the shaft air bearings. In order to obtain any data over a reasonable shaft rundown time, it was necessary to carefully accelerate the shaft to the starting speed of from 200 to 300 rpm and see if the rotation was stable before data were taken. This procedure was successful as the slope confidence interval shows (Table I, p. 24). Although the experimental work was preliminary in nature, it appears unlikely that the large discrepancies indicated in Figure 13 for positive wall Reynolds numbers were introduced by the experimental apparatus. It is speculated that

---

4. Similar instability was also noted for negative Reynolds numbers at starting shaft speeds above about 300 rpm.

an instability phenomenon similar to Taylor vortices exists. A qualitative

justification for this speculation follows. The critical Taylor number (6) is an

indication of vortex formation:

$$T_a = \frac{Wh}{\nu} \sqrt{\frac{h}{r}} \ , \tag{32}$$

wh re W is the peripheral shaft speed, h is the annulus gap, r is the rotating

shaft radius, and ν is the kinematic viscosity of the fluid.

In the present work the maximum shaft peripheral speed was 19.1 in.

per second. This shaft speed resulted in a critical Taylor number of 8.38 and

would indicate a stable condition at least for $R = 0$. The critical Taylor

number could not be calculated for positive or negative wall Reynolds number

since Taylor assumed the radial velocity component to be zero; however, the

circumferential velocity distribution in the radial direction indicates that the

formation of Taylor vortices is plausible. Figure 14 is a graph of the cir-

cumferential velocity distribution in the radial direction for both positive and

negative wall Reynolds numbers. The velocity distribution for positive wall

Reynolds numbers appears similar (for over 50 percent of the gap) to what

could be expected for concentric rotating cylinders with a larger radial

clearance that was used. The critical Taylor number varies as the gap to the

3/2 power of the radial clearance according to equation (32). These consid-

erations indicate that the critical Taylor number quite possibly was reached

for positive wall Reynolds numbers. On the other hand, the same kind of

34
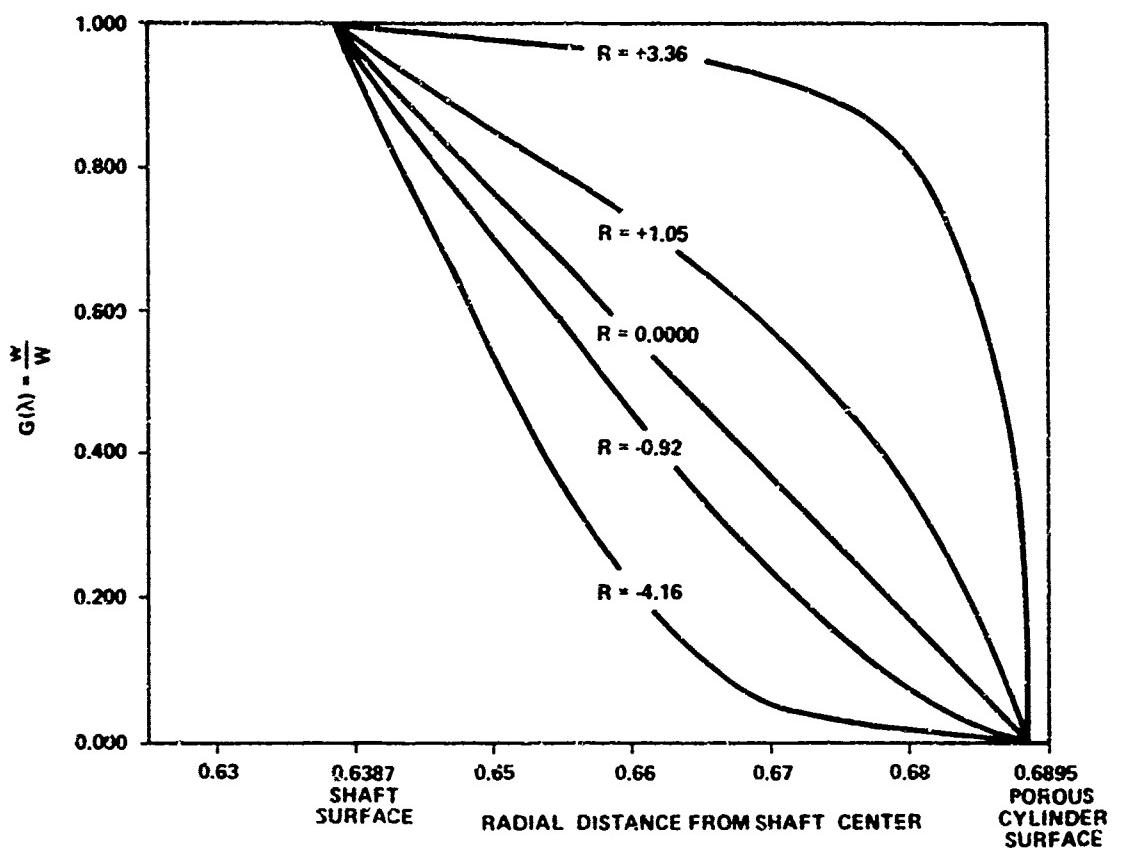
Figure 14. Velocity distribution in annulus.

speculation would predict stability for negative wall Reynolds numbers since

the velocity distribution appears similar to what would be expected with a

much smaller gap.

CHAPTER IV

SUMMARY AND RECOMMENDATIONS

A. Summary

The present work addressed the problem of using a plane channel approximation to obtain theoretical expressions for the drag forces associated with a shaft rotating in a porous cylinder with fluid injection, negative Reynolds numbers, or fluid withdrawal, positive Reynolds numbers. The solution to the Navier-Stokes equations for fluid flow in the axial and radial direction was shown to be independent of the rotational motion of the shaft when the plane channel approximation is used: it predicted the linear relationship of $\ell n \dfrac{\tau_0}{\tau}$ with time in "coastdown" experiments.

A statistical analysis of the preliminary test results confirmed the above linearity. The experimental data agreed reasonably well with the theoretical predictions for negative wall Reynolds numbers; however, the experimental data for positive wall Reynolds numbers did not agree with the theoretical predictions. It was speculated that the lack of agreement between theoretical and experimental results for positive wall Reynolds numbers was due to an instability similar to the formation of Taylor vortices. However, the stiffness properties of the shaft support air bearing (and associated shaft instability) seemed to be such that any disturbance (e. g., hydrodynamic

instability) external to the shaft would preclude stable rotation of the shaft. This possibility is considered in the following section on recommendations for future work.

B. Recommendations

The experience gained during this work and the experimental results suggest a continuation of this work in the positive wall Reynolds number region. A lack of agreement between theory and experiment was shown for positive Reynolds numbers; the shaft support design was not suitable for further investigation of possible causes. e. g.. the previously mentioned speculation on Taylor vortex formation. The use of precision instrument bearings exibiting low constant drag would result in a stiff shaft suspension system that would allow operating speed in excess of 1000 rpm (much higher than our present 300 rpm maximum). Such higher speeds would allow an investigatic of the drag in the vicinity of the critical Taylor number. Additionally. precision instrument bearings would insure that an axisymmetric condition exists between the shaft and the porous cylinder. A small gap h would delay the onset of Taylor vortices; however, a porous cylinder with a more uniform diameter than the one used in this work (0.003 in. out of round with a 0.050-in. annular gap) would be necessary.

The plane channel approximation applied to the case of a shaft rotating concentrically in a porous cylinder predicted a lessening of the drag on the

38

shaft when fluid is withdrawn through the porous cylinder. It would be interesting to investigate further whether there are, indeed, any conditions for which this theoretical prediction could be confirmed by experiment to the same extent as the present work has confirmed the predictions for fluid injection.

LIST OF REFERENCES

39

REFERENCES

1. Berman, A. S., "Laminar Flow in Channels with Porous Walls," J. Appl. Phys, 24, 1232 (1953).

2. Berman, A. S., Paper No. P/720, Proceedings of the Second International Congress for Peaceful Use of Atomic Energy (1958).

3. Terrill, R. M., "Flow Through a Porous Annulus," Appl. Sci. Res., 17, 204 (1967).

4. Terrill, P. M., and Shrestha, G. M., "Laminar Flow Through a Channel with Uniformly Porous Walls of Different Permeability," Appl. Sci. Res., A15 440 (1965).

5. Tsai, M. S., "Laminar Flow in Plane Channel and Annulus with One Wall Porous," Report EM 68-12-1, Department of Engineering Mechanics, University of Tennessee, December 1968.

6. Schlichting, H., Boundary-Layer Theory, Sixth edition (McGraw-Hill Book Co., Inc., New York, 1968), p. 500.

7. Angel, H. R., "Mass Moment of Inertia," Machine Design, May 23, 1968.

APPENDIX

41

APPENDIX

A. Shaft Moment of Inertia

Equation (30) indicates that the moment of inertia should be known precisely in order that G'(0) be determined accurately from the experimental value. The shaft inertia was determined with the aid of two methods.

1. The shaft dimensions were held rigidly during machining and the final dimensions were known precisely. This information, along with a weight measurement of the shaft, was used to calculate the mass moment of inertia of the shaft.

2. The shaft moment of inertia was determined experimentally with the aid of a method by H. M. Angel (7). The shaft was suspended by three strings and caused to oscillate about its longitudinal axis. The weight of the shaft, the suspension string length, the shaft radius and the period of oscillation were used to calculate the moment of inertia of the shaft. The equation used is $J = \frac{WR^2 P^2}{4\pi^2 L}$, where J is the mass moment of inertia of the shaft in in. $-lb_f-sec^2$. W is the shaft weight in pounds, P is the oscillation period in seconds, and R and L are the suspension radius and length, respectively. A typical trial resulted in these data:

$$W = 0.5105 \text{ lb}_f$$
$$R = 0.7320 \text{ in}$$
$$P = 0.5226 \text{ sec}$$
$$L = 4.5 \quad \text{in.}$$

and a J of 4.209×10^{-4} in.-lb_f-sec^2. A small ring used to support the shaft had a calculated value of 0.135×10^{-4} in.-lb_f-sec^2. The resulting shaft mass moment of inertia was 4.074×10^{-4} in.-lb_f-sec^2. The calculated value as determined by item 1. above was 4.130×10^{-4} in.-lb_f-sec^2 or a difference of 0.056×10^{-4}. This represents a possible error in measurement of less than 2 percent.

B. Sample Calculations

1. The wall Reynolds number can be expressed by the following:

$$R = \frac{h\dot{m}}{\mu A} .$$

A typical calculation using the condition imposed on run 60-1 is

$$h = 0.0508 \text{ in.}$$

$$\dot{m} = 0.0036317 \text{ lb}_m/\text{sec}$$

$$\mu = 1.0133 \times 10^{-6} \text{ lb}_m/\text{in.-sec}$$

$$A = 54.208 \text{ in.}^2$$

$$R = 3.3587 .$$

2. The values for $G'(0)$ were calculated from the experimental data. A typical calculation using the data from run 60-1 is

$$G'(0) = \frac{J}{K_1} \text{ (experimental slope)} = 1.5656$$

$$\text{Experimental slope} = -0.0039/\text{sec}.$$

$$K_1 = 1.01475 \times 10^{-6} \text{ in-lb}_f\text{-sec}$$

$$J = 4.074 \times 10^{-4} \text{ in-lb}_f\text{-sec}^2 \ .$$

3. The critical Taylor number may be expressed by the following:

$$T_a = \frac{Wh}{\nu} \sqrt{\frac{h}{r}} = 41.3 \ .$$

Run 55.1 data may be used for this calculation and are

$$W = 19.1 \text{ in./sec}$$

$$r = 0.0386 \text{ in.}$$

$$h = 0.0508$$

$$\nu = 0.03267 \text{ in.}^2/\text{sec} \ .$$

The resulting Taylor number with these data is 8.376.

C. Statistical "Lack-of-Fit-Test"

An F-test was conducted on the data to test the hypothesis that the experimental results were in good agreement with the theoretical predictions for $G'(0)$. This test used the ratio of the sample variance of the theoretical and experimental values of $G'(0)$ and the properly weighed sample variance of the snaft rundown data. The results of the test indicated that the differences between the theoretical and experimental values of $G'(0)$ (Figure 13, p. 31) for our ranges of "r   sonable agreement" are not due to random experimental errors in the rundown data. Sources of experimental bias in

the apparatus (which was not originally designed for shaft rotation) were, of

ccurse, expected. The magnitude of such bias is perhaps indicated by the

difference between the results for clockwise and counterclockwise shaft

rotation.